Kalman Filter-Based Super-Twisting Sliding Mode Control of Shunt Active Power Filter for Electric Vehicle Charging Station Applications

Çelik, Doğan; Ahmed, Hafiz; Meral, Mehmet Emin

IEEE Transactions on Power Delivery

DOI:
https://doi.org/10.1109/TPWRD.2022.3206267

Published: 13/09/2022

Peer reviewed version

Kalman Filter-Based Super-Twisting Sliding Mode Control of Shunt Active Power Filter for Electric Vehicle Charging Station Applications

Doğan Çelik, Hafiz Ahmed, *Senior Member, IEEE*, and Mehmet Emin Meral

***Abstract*—Electric vehicle (EV) charging stations draw nonlinear currents, which makes the distribution network unbalanced, distorted, and results in power quality (PQ) issues. These PQ issues are mitigated in this work through high-performance control of the shunt active power filter (SAPF). In the proposed method, a linear Kalman filter (LKF) has been applied to grid voltage and load current signals for harmonic and disturbance robust estimation purpose. Unlike the conventionally used orthogonal vector model, in this work, phase angle vector model together with a simple to tune phase-locked loop (PLL) has been considered for the LKF implementation. DC-link voltage regulation and charging of the DC-link capacitor has been obtained by proposing a Luenberger observer-based super twisting sliding mode control (ST-SMC), which has fast dynamic response and lower voltage ripples compared to similar other existing control methods. This results in significant reduction in size, cost and loss together with lifetime enhancement of the DC-link capacitor. Rigorous sensitivity analysis is conducted to analyze the robustness of the developed method. The proposed control technique achieves fast response time and satisfy the harmonic requirements as specified in the IEEE Std. 519 under various grid and load disturbances. Comparative quasi-real time validation results are presented by using digital signal processor (DSP) based processor-in-the-loop (PIL) with another recently proposed control strategy to verify the performance enhancement by the developed method.**

***Index Terms*—Power Quality; EV Charging; Shunt Active Power Filter.**

NOMENCLATURE

DSP	Digital Signal Processor
DROGI	Dual Reduced-Order Generalized Integrator
EV	Electric Vehicle
FIR	Finite Impulse Response
FFPS	Fundamental Frequency Positive Sequence
LKF	Linear Kalman Filter
MPC	Model Predictive Control
MCCF	Multiple Complex Coefficient Filter
NLLs	Nonlinear Loads
PLL	Phase-Locked Loop
PCC	Point of Common Coupling
PQ	Power Quality
PIL	Processor-in-the-Loop
PID	Proportional Integral Derivative
PI	Proportional-Integral
STF	Self-Tuning Filter
SAPF	Shunt Active Power Filter
ST-SMC	Super-Twisting Sliding Mode Control
TOSI	Third-Order Sinusoidal Integrator
THD	Total Harmonic Distortion
UNLLs	Unbalanced NLLs
V2G	Vehicle to Grid
+ and -	Positive and Negative Sequence, Respectively
ω	Grid Frequency
V	Voltage Amplitude
T_s	Sampling Time
n	Sampling instants
ζ	State Vector
$\mathcal{P}$	Covariance Matrix
$\mathcal{K}$	Kalman Gain Matrix
$P^\star$	Reference Active Power
P_l	Load Power
σ	Sliding Surface
α and β	Tuning Gains
v_{dc}	DC-link voltage
I_{La}, I_{Lb}, I_{Lc}	Load Phase Currents
v_{LL}	Line to Line PCC Voltage
m	Modulation Index
a	Overloading Factor
I_s	Supply Phase Current
V_{ph}	Supply Phase Voltage
f_s	Switching Frequency
c	DC-link capacitor
$\mathcal{Q}$ and $\mathcal{R}$	Process and Measurement Noise Matrix
$\mathcal{A}$ and $\mathcal{C}$	State and Output Matrix

D. Çelık and M. E. Meral are with the Department of Electrical and Electronics Engineering, Van Yuzuncu Yıl University, Van 65080, Turkey. E-mail: {dogancelik,emeral}@yyu.edu.tr.
H. Ahmed is with the Nuclear Futures Institute, Bangor University, Bangor LL57 2DG, UK (e-mail: hafiz.h.ahmed@ieee.org).
Corresponding Author: H. Ahmed, Address: Nuclear Futures Institute, Bangor University, Bangor LL57 2DG, UK. E-mail: hafiz.h.ahmed@ieee.org; Phone: +44(0)1248 382330.

This work has been supported in part by Van Yuzuncu Yil University Scientific Research Projects Coordination Unit (Van, Turkey) (Project number: FYD-2021-9636). The work of H. Ahmed is funded through the Sêr Cymru programme by Welsh European Funding Office (WEFO) under the European Regional Development Fund (ERDF).

I. INTRODUCTION

The rapidly growing integration of electric vehicle (EV) charger and charging stations in the distribution grid have resulted in a serious concern on power/current quality of the system. EVs battery charging units create destructive effects on the harmonic levels of the power distribution system, voltage profile, power demand and transformer power loss. The increasing distorted current and voltage waveforms result

in heating and losses, affect the lifetime of distribution and instrument transformers and lead to failure of the sensitive electrical equipment. Therefore, it is essential to reduce the possible impact of EV battery charging on distribution power systems [1]–[3]. The power sources of the EVs and plug-in hybrid EVs (PHEVs) are completely or partly supplied from the public power line or on-board chargers, which is fundamentally AC/DC converter. To mitigate the negative effects caused by these AC/DC converters, application of shunt active power filter (SAPF) is suggested in the literature [4], [5]. SAPF coupled with high-performance control system has the potential to lower the total harmonic distortion (THD) of the grid voltages and currents. This motivated us to consider the present study where efficient control of SAPF is studied to facilitate large-scale integration of EV charging stations without compromising the power quality (PQ) issues at the distribution network.

Owing to the importance of SAPF on improving the PQ issues at the distribution network, several control methods are proposed in the literature. Traditionally, SAPF is controlled by controlling the current itself. Any control method for SAPF has typically two parts, namely the reference current generation method and the current controller itself. In [6], for the reference current, a frequency non-adaptive low-pass filter (LPF) approach is considered. LPF makes the system slowly responsive. Moreover, since no frequency adaptation is considered, it can make the performance degrade when the grid undergoes large variation. A proportional-integral (PI) control solution has been proposed for SAPF in [7], where LPFs are used to generate harmonic robust current references. However, the filters are tuned for fundamental frequency operation, which makes the method sub-optimal in the case of grid frequency variation. Moreover, no details are given about the considered phase-locked loop (PLL). PLL tuning plays a big role in weak grid operation of the SAPF. PI controller with parallel harmonic compensation method has been proposed in [8]. This kind of method can be computationally expensive due to the use of numerous parallel harmonic compensation blocks. Moreover, discretization of these blocks can be problematic and may cause numerical issues.

A self-tuning filter (STF) as the reference current generator for SAPF is proposed in [9]. A key limitation of this approach is that the reference generator is not grid frequency-adaptive, thereby, making it vulnerable to fluctuations in the grid frequency. Authors in [10] proposed a modified hysteresis control strategy, however, no validation in the case of unbalanced grid voltages can be found. This can be limited in practice as distributions grid always have some degree of unbalance. In [11], $\mathcal{H}_\infty$ control strategy has been proposed for SAPF. A key limitation of this approach is the selection of weighting functions which requires careful iteration procedures as highlighted in [11]. In [12], an optimization-based approach has been presented to use EV as APF from the power system view point. In [13], PI with feed forward of the grid frequency has been used for controlling the APF. The use of inductor value directly in the feed forward makes this method vulnerable to parameter variation, which is often inevitable due to aging and degradation of the filter inductor. In [14], a dual second-order generalized integrator (DSOGI) has been used to improve the power quality of synchronous generator using APF. In this method, multiple parallel harmonic compensators are used for the reference current generation which increases the computational complexity. To address the grid voltage unbalance and harmonics, a dual third-order sinusoidal integrator (TOSI) is used as the reference generator in [15]. Despite being harmonic robust, the use of PI-type loop filter can slow down the convergence speed for the reference current generation method. Repetitive control method has been applied to SAPF in [16]. However, the results in [16] can not handle unbalanced grid voltage, which limits it's application in practice. A dual reduced-order generalized integrator (DROGI) has been applied in [17]. It uses PI controller for the DC-link voltage regulation which is slowly responsive. This has been tackled by the backstepping method in [18] which requires an estimate of the approximate switching loss. Although this method is robust, however, speeding up the convergence time is not straightforward. As an alternative to PI, fuzzy logic has been considered in [19].

In [20], a sliding mode power control strategy has been developed for SAPF, however, the reference power was generated using a proportional-integral (PI) controller which suffers from the slow dynamic response. Moreover, a conventional phase-locked loop (PLL) is used as the reference current generator which is not able to provide a satisfactory response in the presence of voltage unbalance. In [21], authors have proposed multiple complex coefficient filter (MCCF)-based PI control of DC-link voltage regulation in SAPF. Similar to several other results, MCCF in [21] is also not frequency-adaptive which limits its application in variable frequency environment. To compensate for the sampling period delay, a finite impulse response (FIR) prediction filter together with the PI DC-link voltage regulation method for SAPF is proposed in [22]. Indirect DC-link voltage control using fuzzy logic tuned proportional-integral-derivative (PID) controller is proposed in [23]. In addition to the implementation complexity of fuzzy-PID (FPID) control, a LPF is also required to filter the measured DC-link voltage which can slow down the dynamic behavior of the resulting control system. Model predictive control (MPC) is another approach that became very popular in recent times. In [24], authors have applied MPC to SAPF. Although the switching pulses of the inverter are generated by the MPC technique, however, the DC-link voltage regulation was done by a PI controller. Moreover, MPC can be sensitive to system parameters variation. In [25], second-order sinusoidal integrator is coupled with frequency-adaptive comb filter to control SAPF. In a variable frequency environment, a frequency-adaptive comb filter is computationally expensive to implement as it requires fractional delay. A comparative assessment of sequence extraction methods can be found in [26].

To address the issues highlighted in the literature review, a high-performance control strategy has been conceived for SAPF that operates as a harmonic compensation device to mitigate the negative impacts caused by the utility grid-interfaced EV charging stations. The conceived strategy performs within the harmonic regulatory limit specified through

IEEE std. 519-2014. The performance has been tested under grid side disturbances (e.g. unbalanced and distorted) as well as load side disturbances such as under highly inductive nonlinear loads (NLLs) and unbalanced NLLs (UNLLs). The proposed controller is developed in two steps. At first, a linear Kalman filter (LKF) has been applied to grid voltage and load current signals for harmonic and disturbance robust estimation purpose. The estimated quantities are used to calculate the reference currents. In the second part, a super-twisting sliding mode controller (ST-SMC) is developed for fast and robust regulation of the DC-link voltage which is then used to generate the reference power for the current controllers. The proposed method is extensively tested and compared with another recent technique [17] from the literature. In addition, a qualitative comparison with the wider literature is also presented. Extensive DSP based PIL quasi real-time results indicate the proposed control method is very effective in suppressing harmonics and can ensure balanced currents irrespective of the disturbances presented in the grid. Key features of the proposed work are:

- Frequency-adaptive sequence components separation of grid voltage and load current signals by the LKF with excellent noise and harmonics robustness property.
- Luenberger observer-based ST-SMC controller development for fast and accurate regulation of DC- link voltage with very low ripple.
- Software-based DC-Link voltage ripple reduction without increasing the hardware rating, thereby increasing the lifetime and reducing the cost.
- Very low THD achieved in the source current resulting in distribution system efficiency enhancement.
- Achieved balanced source currents irrespective of grid voltage conditions resulting in the efficient operation of the power grid.
- Sensitivity analysis of the developed system has been derived with respect to system parameters filter inductor and DC-link capacitor.
- Robustness of the developed control system has been investigated subject to uncertainties in system parameters.

In short, this work proposed a high-performance control algorithm for the SAPF used in EV charging station. As opposed to recently proposed control methods in the literature, the proposed controller ensures fast dynamic response with enhanced steady-state performance in terms of significant reduction in the DC-link capacitor voltage. It provides an easy to implement solution that can significantly reduce the THD resulting in efficiency improvement of the distribution system. It can seamlessly handle grid and load side disturbances such voltage sag, unbalance, and/or harmonic distortion. and improves the efficiency of distribution system. The first key novelty of this work is the development of Luenberger observer-based ST-SMC for maintaining constant voltage at the SAPF's DC-link. Second novelty use the development of LKF based filtering of grid voltage and load currents using phase angle vector model. Coupled with a fast and easy to tune PLL, this approach contributed to harmonically robust generation of reference currents. Another key focus of this work is to couple SAPF with bidirectional DC-DC converter to charge the EV battery packs, which made the proposed system multi-functional.

This paper is organized as: Details of the LKF based sequence components separation process is given in Sec. II, Luenberger observer-based ST-SMC control method for the DC-Link voltage regulation together with components selection for the SAPF are given in Sec. III. Comparative PIL based quasi *real-time* results are provided in Sec. IV. Concluding remarks can be found in Sec. V.

II. Kalman Filter-Based Sequence Component Separation

Kalman filter is a very popular tool in the literature for state estimation of dynamical systems with noisy measurements. It has a real-time implementation friendly recursive structure. It can provide optimal estimation from inaccurate and uncertain measurements. In the case of our application, we need to extract the fundamental frequency positive sequence (FFPS) component from the unbalanced three-phase grid voltage and load current signals. Since the grid voltages and load currents are a combination of sinusoidal signals, LKF can be used to efficiently extract the FFPS component from the measured noisy and potentially harmonically distorted signals. In the following, only the separation of grid voltages FFPS components are discussed. Separation of load currents can be done in the same manner. As such, it will not be discussed in details for the sake of brevity. For further development, let us consider the stationary reference frame $(\alpha-\beta)$ model of the voltage signals:

$$v_\alpha(t) = v_\alpha^+(t) + v_\alpha^-(t) = V^+\cos(\theta^+) + V^-\cos(\theta^-), \quad (1)$$

$$\begin{aligned} v_\beta(t) &= v_\beta^+(t) + v_\beta^-(t), \\ &= V^+\cos\left(\theta^+ - \pi/2\right) - V^-\cos\left(\theta^- - \pi/2\right), \end{aligned} \quad (2)$$

where the superscript $+$ and $-$ indicate the positive and negative sequence components, V denote the amplitude, instantaneous phases are defined by $\theta^+ = \omega t + \phi^+$ and $\theta^- = \omega t + \phi^-$ where the grid angular frequency is ω and the initial phase angles are ϕ^+ and ϕ^-. Using trigonometric expansion, equations (1) and (2) can be expanded as:

$$v_\alpha(t) = \xi_1\cos(\omega t) + \xi_2\sin(\omega t), \quad (3)$$

$$v_\beta(t) = \xi_3\cos(\omega t - \pi/2) + \xi_4\sin(\omega t - \frac{\pi}{2}), \quad (4)$$

where $\xi_1 = V^-\cos(\phi^-) + V^+\cos(\phi^+)$, $\xi_2 = -(V^-\sin(\phi^-) + V^+\sin(\phi^+))$, $\xi_3 = -(V^-\cos(\phi^-) - V^+\cos(\phi^+))$, and $\xi_4 = V^-\sin(\phi^-) - V^+\sin(\phi^+)$. From equations (3) and (4), let us consider the state vector as $\boldsymbol{\xi} = \begin{bmatrix} \xi_1 & \xi_2 & \xi_3 & \xi_4 \end{bmatrix}^T$. With respect to $\boldsymbol{\xi}$, the dynamic model of Clarke transformed grid voltages is given by:

$$\dot{\boldsymbol{\xi}} = \mathcal{A}\boldsymbol{\xi}, \quad (5)$$

$$\boldsymbol{y_\xi} = \mathcal{C}\boldsymbol{\xi}, \quad (6)$$

where $\boldsymbol{y_\xi} = [v_\alpha(t); v_\beta(t)]$ is the output vector, $\mathcal{A} \in \mathbb{R}^{4\times4}$ and $\mathcal{C} \in \mathbb{R}^{2\times4}$ are the state and output matrices and given below:

$$\mathcal{A}=\begin{bmatrix}1&0&0&0\\-1&0&0&0\\0&0&1&0\\0&0&-1&0\end{bmatrix},\mathcal{C}=\begin{bmatrix}\cos(\omega t)&0\\\sin(\omega t)&0\\0&\cos(\omega t-\frac{\pi}{2})\\0&\sin(\omega t-\frac{\pi}{2})\end{bmatrix}^{T}$$

For recursive digital implementation, let us consider that $t=nT_s, n=\overline{0,N}$ where sampling instant and time are denoted by n and T_s. By applying exact-discretization to the matrices A and C, one can obtain that $\mathcal{A}(n)=\exp(\mathcal{A}T_s)\approx I_4$ and

$$\mathcal{C}(n)=\begin{bmatrix}\cos(\omega nT_s)&\sin(\omega nT_s)&0&0\\0&0&\cos(\Omega_n)&\sin(\Omega_n)\end{bmatrix},$$

where $\Omega_n=\omega nT_s-\frac{\pi}{2}$, I_4 is the identity matrix of dimension 4×4. Discrete-time model of (5) and (6) by considering the process and measurement noises are given by:

$$\boldsymbol{\xi}(n+1)=\mathcal{A}(n)\boldsymbol{\xi}(n)+\varpi(n), \tag{7}$$

$$\boldsymbol{y_\xi}(n)=\mathcal{C}(n)\boldsymbol{\xi}(n)+\nu(n), \tag{8}$$

where process and measurement noise $\varpi(n)$ and $\nu(n)$ are not correlated and zero-mean Gaussian white noise with $\mathbb{E}\left(\varpi(n)^T\varpi(n)\right)=\mathcal{Q}(n)=qI_4, q>0$ and $\mathbb{E}\left(\nu(n)^T\nu(n)\right)=\mathcal{R}(n)=rI_2, r>0$ being the process and measurement noise covariance matrices of appropriate dimensions. In developing model (7) and (8), it is assumed that the frequency ω in the output matrix $C(n)$ is known for the sake of simplicity. Here, we are using a phase-locked loop (PLL) [27] for unknown frequency estimation that is then feedback for the output matrix calculation. For a model (7) and (8), the recursive implementation of the conventional Kalman filter by taking into account the special property of the state transition matrix is given below:

$$\hat{\boldsymbol{\xi}}(n|n-1)=\hat{\boldsymbol{\xi}}(n-1|n-1), \tag{9}$$

$$\mathcal{P}(n|n-1)=\mathcal{P}(n-1|n-1)+\mathcal{Q}(n), \tag{10}$$

$$\mathcal{K}(n)=z(n)\left(\hat{\mathcal{C}}(n)\mathcal{P}(n|n-1)\hat{\mathcal{C}}^T(n)+\mathcal{R}(n)\right)^{-1}, \tag{11}$$

$$\hat{\boldsymbol{\xi}}(n|n)=\hat{\boldsymbol{\xi}}(n|n-1)+\mathcal{K}(n)\left(\boldsymbol{y_\xi}(n)-\hat{\mathcal{C}}(n)\hat{\boldsymbol{\xi}}(n|n-1)\right), \tag{12}$$

$$\mathcal{P}(n|n)=\left(I_4-\mathcal{K}(n)\hat{\mathcal{C}}(n)\right)\mathcal{P}(n|n-1), \tag{13}$$

where $z(n)=\mathcal{P}(n|n-1)\hat{\mathcal{C}}^T(n)$, $\hat{}$ specifies the estimated quantity, n is the discrete-time index, *a priori* and *post priori* estimates are denoted by $n|n-1$ and $n|n$, covariance matrix is denoted by $\mathcal{P}$ with $\mathcal{P}(0)=pI_4, p>0$, and $\mathcal{K}\in\mathbb{R}^{2\times 4}$ is the Kalman gain matrix. From the estimated states $\hat{\boldsymbol{\xi}}$, fundamental frequency positive sequence DC components can be estimated as:

$$\hat{\xi}_s^+=-\frac{1}{2}\left(\hat{\xi}_2+\hat{\xi}_4\right)=\hat{V}^+\sin\left(\hat{\phi}^+\right), \tag{14}$$

$$\hat{\xi}_c^+=\frac{1}{2}\left(\hat{\xi}_1+\hat{\xi}_3\right)=\hat{V}^+\cos\left(\hat{\phi}^+\right). \tag{15}$$

Then, from the estimated signals (14) and (15), grid parameters can be estimated as:

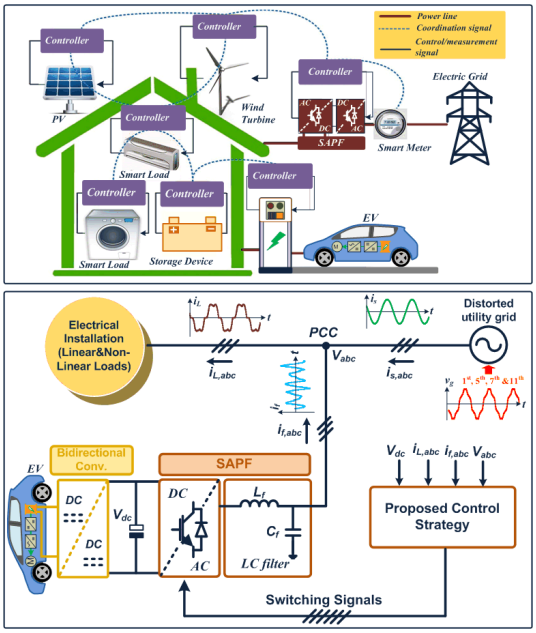

Figure 1. Schematic of (a) smart loads and EV charging station with the compensator installation and (b) the SAPF system under study.

$$\hat{\phi}^+=\text{atan2}\left(\hat{\xi}_s^+,\hat{\xi}_c^+\right), \tag{16}$$

$$\hat{V}^+=\sqrt{\left(\hat{\xi}_s^+\right)^2+\left(\hat{\xi}_c^+\right)^2}. \tag{17}$$

The detected phase angle can be used for PLL implementation [27]. From the PLL, the instantaneous phase can be estimated as:

$$\hat{\theta}^+=\hat{\omega}t+\hat{\phi}^+. \tag{18}$$

Using the estimated instantaneous phase and the amplitude, the positive sequence component can be estimated as:

$$\hat{v}_\alpha^+(t)=\hat{V}^+\cos\left(\hat{\theta}^+\right), \tag{19}$$

$$\hat{v}_\beta^+(t)=\hat{V}^-\sin\left(\hat{\theta}^+\right). \tag{20}$$

III. Proposed Control Strategy for Power Quality Improvement

An overview of the considered system is given in Fig. 1. Control algorithm decides the appropriate compensation current generation by the SAPF so that the current drawn for the grid has low THD satisfying the appropriate standards. The proposed control strategy is made of DC-link voltage control and the calculation of reference current. Once the reference current is generated, conventional current controllers will be used to generate the PWM signals for SAPF. Details of the considered system and the developed control technique together with the selection of the system parameters are provided in this Section.

A. Details of the Considered EV Charging Station

Fig. 1 shows the considered EV charging station, which is linked to the point of common coupling (PCC) between the

power grid and the electrical installation loads (linear loads and NNLs). The grid connected EV charging station includes a control unit, DC-link capacitor, bidirectional DC-DC and DC-AC converters. The EV charger has a front-end DC/AC converter that connects to the back-end DC/DC converter through a DC-link capacitor. The EV charger is integrated to the electric grid through a passive filter (L_f and C_f) at the front-end while it is tied with EV batteries at the back-end. The EV battery charger takes power from the grid and charges the on-board EV battery pack. Besides, bidirectional chargers can fulfill vehicle to grid (V2G) operation and other grid supporting features such as reactive compensation and harmonic compensation as well as EV battery charging. An EV charger can work as a multi-functional APF to mitigate the harmonics and handle the voltage disturbances as a result of motor startup or inductive loads and NNLs at the local network. The DC/AC converters or SAPF ensuring the power flows between grid, load and EVs are commonly designed to deal with the PQ problems and support the grid. The EV motor driver is made with a three-phase inverter, as induction or permanent magnet synchronous motors are often used for EVs. In this regard, the three-phase inverter of the EV powertrain can be adapted to the application of an APF. A potential area for the implementation of SAPF in residential and commercial power grids could be realized through the use of on-board converters of the EVs, as reported in [12], [13], [28]–[30]. In this context, intensive application of APFs in residential and commercial facilities can be a way to reduce PQ problems in distribution networks, reduce losses, decrease the total harmonic distortion and reactive power flows and increase active power transmission capacity within the electrical feeders.

B. Observer-based Super-Twisting Sliding Mode DC-link Voltage Control

Maintaining the DC-link voltage at a fixed value is essential for effective operation of the SAPF. This will contribute to the appropriate sinusoidal current generation by the inverter. Various losses affect the operation of the SAPF such as switching and output filter loss. As such, constant DC-link voltage will ensure that appropriate peak value of the reference current can be tracked. For this purpose, sliding mode control strategy [31]–[33] is considered in this work. To develop the controller, let us assume that the SAPF is operating in a well-controlled manner. Moreover, switching losses are also ignored. Then, according to the power balance theory, one can write that:

$$P^{\star} - P_l = \frac{c}{2}\frac{d}{dt}\left(\frac{v_{dc}^2}{2}\right), \tag{21}$$

where the DC-link capacitor and voltage are denoted by c and v_{dc}, $P^{\star}$ is the reference active power, and P_l is the load power. Let us consider that $\zeta_1 = 0.5v_{dc}^2$ and $\zeta_2 = P_l$. Then, from eq. (21), the following DC-link dynamical model is obtained:

$$\dot{\zeta}_1 = 2\left(P^{\star} - \zeta_2\right)/c, \tag{22}$$

$$\dot{\zeta}_2 = f\left(\zeta, t\right), \tag{23}$$

$$y_{\zeta} = \zeta_1, \tag{24}$$

where the load power dynamics is given by the function $f\left(\zeta, t\right)$ with ζ being the state vector containing ζ_1 and ζ_2 and the output is the measured DC-link voltage.

1) Super-Twisting Control: To design the DC-link voltage regulator, let us select the following sliding surface σ:

$$\sigma = \zeta_1^{\star} - \zeta_1, \tag{25}$$

where the target value is denoted by $\star$. By differentiating (25), one can obtain that:

$$\dot{\sigma} = \frac{2}{c}\left(\zeta_2 - P^{\star}\right). \tag{26}$$

According to the super-twisting SMC results presented in [31]–[33], the control signal u can be calculated as:

$$u = u_{eq} + U_{ST}, \tag{27}$$

where u_{eq} is the equivalent control which is obtained by setting $\dot{\sigma} = 0$ and the super-twisting part u_{ST} can be chosen as:

$$u_{ST} = \alpha\lfloor\sigma\rceil^{\frac{1}{2}} + \beta\int_0^t \lfloor\sigma\rceil^0 dt, \tag{28}$$

where the positive constants α and β are tuning gains, and $\lfloor\cdot\rceil^{\eta} = |\cdot|^{\eta}\text{sign}\left(\cdot\right), \eta \geq 0$. Then, by using eq. (28) and the equivalent control signal from $\dot{\sigma} = 0$, the DC-link control signal which is the reference power $P^{\star}$ can be calculated as:

$$P^{\star} = \zeta_2 + \alpha\lfloor\sigma\rceil^{\frac{1}{2}} + \beta\int_0^t \lfloor\sigma\rceil^0 dt. \tag{29}$$

Control signal (29) requires the state ζ_2 which is the load power. This signal is not available in practice. As such an estimator needs to be designed for this purpose and detailed in Sec. III-B2. With respect to the estimated load power, control (29) can be rewritten as:

$$P^{\star} = \hat{\zeta}_2 + \alpha\lfloor\sigma\rceil^{\frac{1}{2}} + \beta\int_0^t \lfloor\sigma\rceil^0 dt. \tag{30}$$

2) Linear Observer : The designed controller requires the estimated state $\hat{\zeta}_2$. To develop an estimator for this, we are considering the model (22)-(24). Let us consider that the load is constant, resulting in $f\left(\zeta, t\right)$ equals to zero in (23). This will simplify the estimator design. To design the linear observer, first, let us put the model (22)-(24) into the state-space form as given below:

$$\dot{\zeta} = A\zeta + Bu, \tag{31}$$

$$y_{\zeta} = C\zeta, \tag{32}$$

where $\zeta = \begin{bmatrix} \zeta_1 & \zeta_2 \end{bmatrix}^T$, $u = P^{\star}$,$A = [0 \ -2/c; 0 \ 0]$,$B = [2/c; 0]$, $C = [1 \ 0]$. Then, for system (31) and (32), the following linear Luenberger observer can be designed:

$$\dot{\hat{\zeta}} = A\hat{\zeta} + Bu + \mathcal{L}\left(y_\zeta - \hat{y}_\zeta\right), \tag{33}$$

$$\hat{y}_\zeta = C\hat{\zeta}, \tag{34}$$

where the appropriately output error correction matrix $\mathcal{L} \in \mathbb{R}^{2\times 1}$ ensures that the closed-loop observer error matrix $A - \mathcal{L}C$ is Hurwitz, i.e., all the eigenvalues of negative real parts. This ensures the asymptotic stability of the observer, consequently asymptotic estimation of the states ζ_1 and ζ_2.

C. SAPF Circuit Parameters Selections

A small size capacitor is an admissible choice to ensure smaller APF size, higher reliability and lower cost. The minimum DC-link voltage is given by:

$$v_{dc,min} = 2\sqrt{2}v_{LL}/(\sqrt{3}m), \tag{35}$$

where modulation index and line to line PCC voltage are specified by m and v_{LL}. Then, the following formula can be used fro DC-link capacitor value calculation:

$$\frac{1}{2}c\left(v_{dc}^2 - v_{dc,min}^2\right) = 3g\left\{V_{ph}(aI_s)t_r\right\}, \tag{36}$$

where $g \in [0.04, 1.15]$, supply phase current and voltages are denoted by I_s and V_{ph}, factor of overloading is denoted by a and DC-link voltage recovery time is t_r. Filter inductance value can be computed by:

$$L_f = \sqrt{3}mv_{dc}/(12af_sI_{cr}), \tag{37}$$

where acceptable percentage output current ripple is given by I_{cr} and power circuit switching frequency is given by f_s. Base value of the AC capacitor of SAPF is given by [34];

$$C_b = P_n/(\omega_f v_{LL}^2), \tag{38}$$

where nominal power of SAPF is P_n and grid frequency is ω_f. From base value, filter capacitor value is calculated as $C_f = xC_b$ where x being percentage of reactive power consumed by the SAPF.

D. Reference Current Generation

The required compensation currents have to be achieved accurately to deal with the PQ issues. The desired currents values are calculated through DC-link controller and LKF based filtering of grid voltage and load currents. The sensed load currents are extracted by the LKF to calculate the necessary compensating current output by the SAPF. Clarke transformation ($\alpha - \beta$) is applied to load currents ($I_{L\alpha}, I_{Lb}, I_{Lc}$) for further processing. Therefore, the converted load currents ($I_{L\alpha}$and$I_{L\beta}$) are separated into positive, negative and harmonic sequence parts as written by:

$$I_{L\alpha} = I_{L\alpha}^{+} + \left\{\sum_{h=2}^{\infty} I_{L\alpha h}^{+} + \sum_{h=1}^{\infty} I_{L\alpha h}^{-}\right\}, \tag{39}$$

$$I_{L\beta} = I_{L\beta}^{+} + \left\{\sum_{h=2}^{\infty} I_{L\beta h}^{+} + \sum_{h=1}^{\infty} I_{L\beta h}^{-}\right\}, \tag{40}$$

where h denotes the number of harmonic components. The compensating currents ($I_{f\alpha,comp}$ and $I_{f\beta,comp}$) of the SAPF are acquired by comparing sensed loads with the fundamental load current components ($\hat{I}_{L\alpha} = I_{L\alpha}^{+}$ and $\hat{I}_{L\beta} = I_{L\beta}^{+}$) as follows:

$$I_{f\alpha,comp} = I_{L\alpha} - I_{L\alpha}^{+} = \sum_{h=2}^{\infty} I_{L\alpha h}^{+} + \sum_{h=1}^{\infty} I_{L\alpha h}^{-}, \tag{41}$$

$$I_{f\beta,comp} = I_{L\beta} - I_{L\beta}^{+} = \sum_{h=2}^{\infty} I_{L\beta h}^{+} + \sum_{h=1}^{\infty} I_{L\beta h}^{-}, \tag{42}$$

Active power can be handled by the output the Luenberger observer based ST-SMC DC-link voltage controller (reference active power, $P^\star$) is multiplied with the sequence units of $\hat{\xi}_c^{+}$ and $\hat{\xi}_s^{+}$to generate active currents or called DC currents ($I_{f\alpha,dc}$ and $I_{f\beta,dc}$) as;

$$I_{f\alpha,dc} = \hat{\xi}_c^{+}P^\star / \left(\hat{\xi}_c^{+}\right)^2 + \left(\hat{\xi}_s^{+}\right)^2, \tag{43}$$

$$I_{f\beta,dc} = \hat{\xi}_s^{+}P^\star / \left(\hat{\xi}_c^{+}\right)^2 + \left(\hat{\xi}_s^{+}\right)^2. \tag{44}$$

Instantaneous active currents can be called the DC currents as they are generated through DC-link controller. Active currents or (DC currents) refers the three-phase currents compensated by the SAPF. The reference active or DC currents of the SAPF are given by using (41)-(44):

$$I_{f\alpha,dc}^{\star} = I_{f\alpha,comp} - I_{f\alpha,dc}, \tag{45}$$

$$I_{f\beta,dc}^{\star} = I_{f\beta,comp} - I_{f\beta,dc}. \tag{46}$$

In this paper, the proportional resonant (PR) controller has been employed to provide current regulation and excellent current tracking behavior as well as restricting the THD value.

$$G_c = K_{ip} + \frac{2K_{ir}s}{s^2 + 2\zeta_r\omega s + \omega^2}, \tag{47}$$

where K_{ip} and K_{ir} represent the proportional and resonant gains, respectively. ζ_r is the damping factor, which can be considered as 0.707 to provide fulfilling tracking performance in the range of (1 ±0.01) fundamental grid frequency [35]. Estimating current errors ($I_{f\alpha,e} = I_{f\alpha,dc}^{\star} - I_{f\alpha}$) and ($I_{f\beta,e} = I_{f\beta,dc}^{\star} - I_{f\beta}$) have been obtained after reference active or DC currents and sensed currents in the output of the SAPF are processed by the PR current controller. Switching signals of the SAPF switches are calculated by estimating current errors and the inverse Clarke transformation. Figure 2 shows the diagrammatic depiction of the developed control method.

IV. Results and Discussion

The developed control strategy is applied in this Section to the SAPF considering the nonlinear load of EV charging station applications. The proposed method is compared to the previous study reported in [17] via DSP based PIL results. Table I lists the considered system and control parameters.

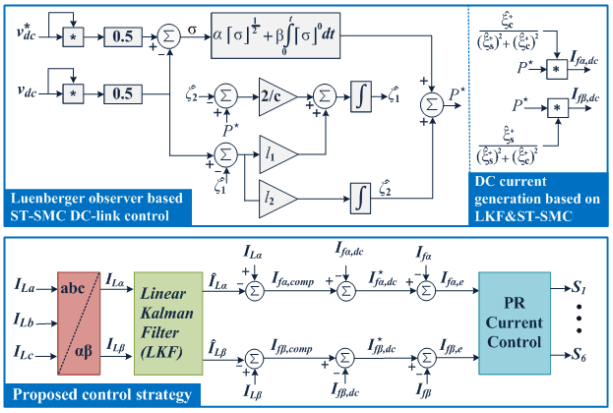

Figure 2. The proposed control strategy.

Table I
THE PROPOSED SYSTEM PARAMETERS.

Description	Parameters	Value
Grid Voltage	v_{LL} (rms)	380V
Grid Freq.	ω	50Hz
Switching Freq.	f_s	10kHz
Sampling Time	T_s	$40\mu s$
SAPF DC-Link	$v_{dc}^{\star}, c$	650V, 3300μF
SAPF Filter	L_f, C_f	5mH, 16μF
LKF	$\mathcal{Q} = 0.05I_4, \mathcal{R} = 0.1I_2$	
Observer	$\mathcal{L} = \begin{bmatrix} 0.1316 & 0.1108 \end{bmatrix}^T$	
ST-SMC	$\alpha = 80$ and $\beta = 5$	

A. DSP based PIL Evaluation

Validation of the control algorithm developed in this work is considered through execution by TMS320F28335 DSP within a PIL in PSIM platform as depicted in Fig. 3. TargetLink code of the developed control method can also run on both the PIL testbench and dSPACE's PC-based simulator. While the PIL test bench operates in semi-real time and achieves a high degree of flexibility in designing a advanced control algorithm, dSPACE tools can be employed for real-time simulation [36]. dSPACE Simulator can execute test automation, monitoring, data acquisition and simulated driving cycles, but its hardware requirements can be very expensive depending on hardware in loop (HIL) applications. On the other hand, the PIL module

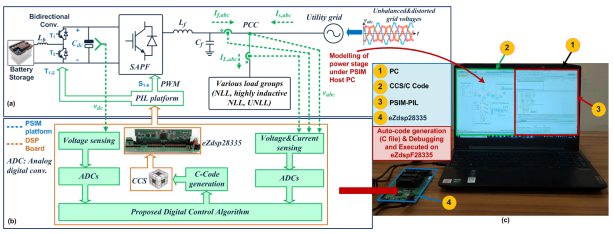

Figure 3. Performance validation setup; a) modeling power stage under PSIM host PC, b) developing the proposed control strategy to generate code (C file) and execute on eZdspF28335 and c) DSP based PIL experiment test platform.

provides an interface between power stages implemented and simulated in PSIM and embedded processor. In this paper, the PIL testbench consists of TMS320F28335 DSP that is interfaced to PSIM environment utilizing a high-speed serial interface unit. The PIL semi-experiment test platform includes hardware and software co-interaction. The C-code is generated by the digital control algorithm and it is linked and compiled with code composed studio (CCS). After that, this code is programmed and run on the DSP hardware, which is interfaced to the PC with USB/JTAG communication.

At 0.225s, line to line to ground (LLG) and line to ground (LG) grid faults with 35% voltage drop have been considered for all experimental cases except for load change to assess the efficacy the proposed control. Figures 4 and 5 display the waveforms of the PCC and DC-link voltage, source and load currents. Fig. 4 shows that the proposed control provides an excellent improvement in harmonic rejection capability and fast dynamic response under NLLs, load change and highly inductive NLLs as opposed to [17]. As found in Fig. 4a, the developed method fulfills the exigencies dedicated by IEEE-519 harmonics standards and also has better performance in mitigating both individual harmonic amplitudes and THD of the source currents (*cf.* Fig. 6). As depicted in the middle of Fig. 4a and 4b, the performance of both control methods have been examined under dynamic load change. The proposed control using ST-SMC achieves an excellent dynamic response within 10ms under load change while the conventional control using PI has a dynamic response of 40ms. Besides, the ripple voltage of the DC-link by the developed technique is lower compared to existing method [17]. Under highly inductive NLL and during grid faults condition, the proposed control's DC-link voltage ripple is $\Delta\hat{v}_{dc} = 1.0V$, while the DC-link voltage ripple is $\Delta\hat{v}_{dc} = 6.43V$ with the conventional control (see the right side of Fig. 4a and Fig. 4b). The proposed control provides sinusoidal source currents with THD of nearly 2.0%, which is within the regulatory limit of IEEE Std. 519-2014. However, the THD value of the conventional control is higher and especially under highly inductive NLL it could not meet the limits of the aforementioned standard. The developed control technique achieved balanced source currents irrespective of the grid condition, which is not the case for conventional method when the grid is unbalanced. Unbalanced currents can introduce currents within the neutral line and voltage imbalance. Thus, the neutral currents induce losses and causes extreme heating. Results show that the developed method outperformed the conventional counterpart in all cases.

Evaluating the performance of the control strategies under UNLL and distorted source voltages, one can notice that the distortions of the current waveforms are higher for the conventional control as seen in Fig. 5a. At 0.15s, the SAPF is connected to the distorted grid with having 5^{th}, 7^{th} and 11^{th} harmonics. The THD of per-phase currents remained below 5% in value by the developed method satisfying the regulatory limit of IEEE Std. 519-2014, the conventional control cannot effectively suppress harmonics within the mandated limit. The proposed control effectively compensates harmonics caused by NLL, UNLL and distorted grid voltage. The DC-link voltage with conventional control has larger ripples. It is obvious

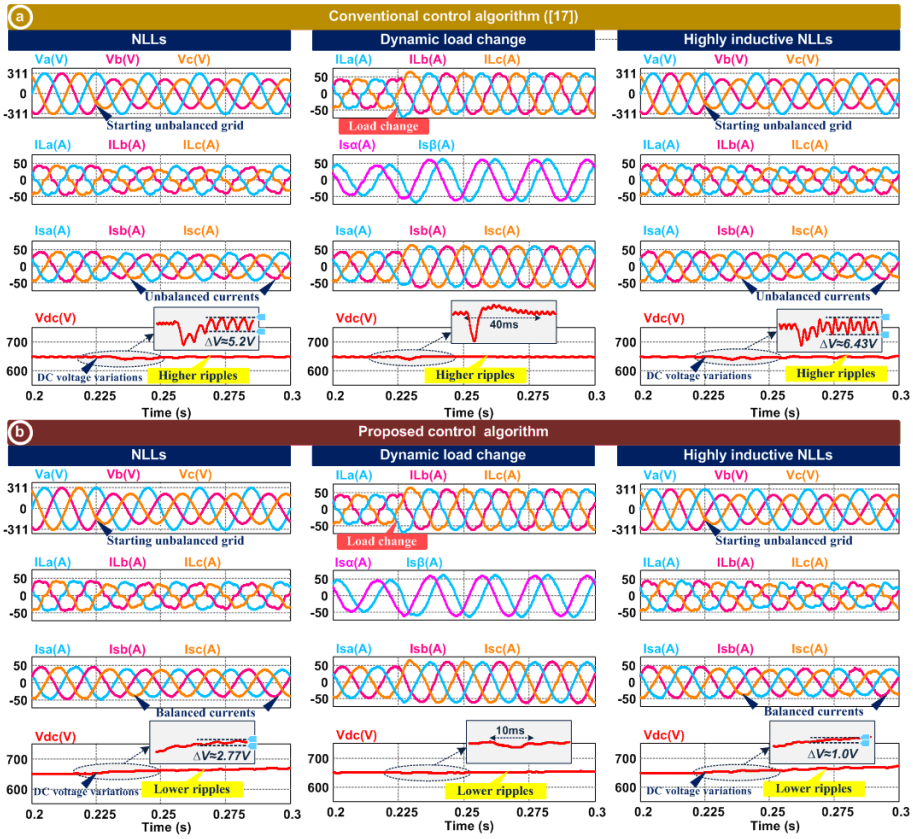

Figure 4. DSP based PIL evaluation with an NLL, load change and highly inductive NLL. (a) existing method [17] and (b) This work.

from Fig. 5b that the ST-SMC provides better performance in the DC-link voltage ripple elimination, providing a reduction in the size of the DC-side capacitor. In addition, balanced sinusoidal source currents are another key features of the developed method unlike the conventional technique.

B. Discussion and Comparison of the Developed Control and the Wider Literature

Fig. 6 presents the current harmonic spectrum for the proposed and conventional control strategies under various case studies. The THD and individual harmonic components values of phase currents are given in Figs. 4 and 5 have been measured between 0.2s-0.3s (100ms, 5 time period for 50Hz). The time window has been selected as it covers both steady-state and dynamic condition, i.e., change in source and load. This can be considered as a representative time window for harmonic robustness analysis. It is evident that the individual harmonic amplitudes and THD value of the source current are significantly lower compared to the conventional counterpart. This makes the proposed method highly suitable to reduce the overall distortions in the grid voltage and currents, thereby improving the power quality of the distributions grid when highly nonlinear loads such as EV charging stations are operational.

Table II presents a summary of the deficiencies in the previous studies based on several important factors. The qualitative analysis based comparison is conducted in regards to reference current generation, DC-link voltage control, THDs of source currents, DC-link voltage ripples and dynamic response. The existing studies didn't focus much on the DC-link voltage control and utilized typically PI or PID controllers. Authors in [18] have presented a backstepping DC-link control, that achieves fast transient response but THD of the source currents are higher. On the other hand, various voltage and current estimation methods such as MCCF [21], reduced order generalized integrator (ROGI) [17], [23], comb filter based SOGI (CF-SOGI) [25] and FIR [22] have been addressed in the previous studies. From the quasi-real time results, the proposed control strategy including ST-SMC DC-link control and voltage-current signal estimation with LKF exhibit superior performance with respect to current harmonics mitigation and convergence speed improvement. This work has achieved a THD level well below the IEEE-519 standard on current harmonics compared to the existing result.

C. Sensitivity Analysis of the System Parameters

The impacts of the SAPF circuit parameters (L_f and c) in the overall control performance can be determined by aspect of the voltage ripple factor, power ripple and current distortion to analyze the costing and sizing of the system and the THD value. The variation of L_f have an impact on the current quality [38]. The changing filter inductance can be given by;

$$\Delta L = (L_f - L_n)/L_n \tag{48}$$

where L_f and L_n represent the actual and nominal filter inductance.

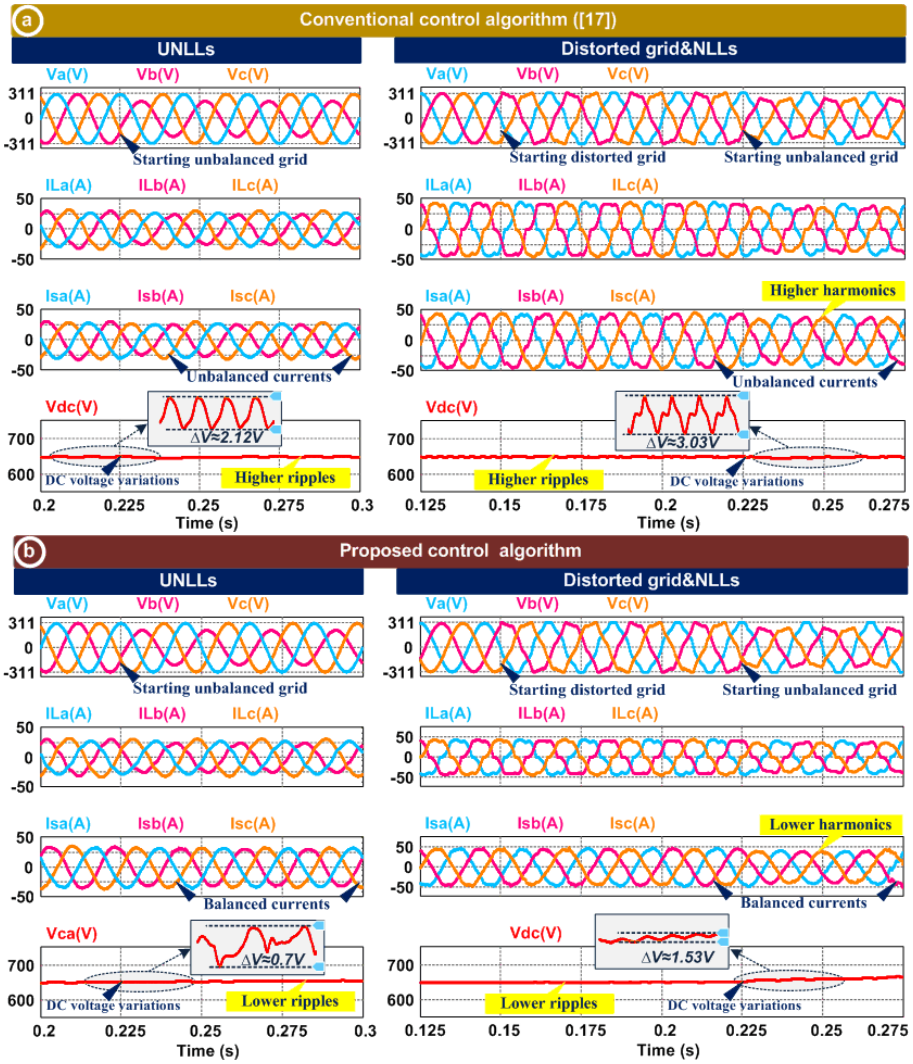

Figure 5. DSP based PIL evaluation of (a) existing method [17] and (b) this work under a UNLL and distorted grid using NLL.

Table II
PROPERTIES COMPARISON WITH THE PREVIOUS CONTROL STRATEGIES.

Method	Voltage & Current Estima-tion	DC-link control	THDs of source currents	DC-link voltage ripples	Dynamic response
[11]	LKF	H_∞	Low	High	Slow
[17]	ROGI	PI	High	High	Slow
[18]	STF	Backstepping	High	Low	Fast
[21]	MCCF	PI	High	High	Slow
[22]	FIR	PI	Low	High	Slow
[23]	ROGI	FPID	Low	Low	Slow
[25]	CF-SOGI	PI	High	High	Slow
[37]	SOGI	PI	High	High	Slow
Proposed	LKF	ST-SMC	Very Low	Very Low	Fast

The voltage ripples in the DC-link have an impact on the lifetime of the capacitor, switching components of the power converters and power losses. Large DC-link capacitor can reduce voltage ripple, but it augment the size, cost and weight of the system. Despite not using large capacitor, the proposed control technique can maintain constant DC-link voltage. To charge the DC-link capacitor, an extra active power must be absorbed by the grid to arrange the DC-link voltage. As the real actual voltage is different from the target voltage, it causes a difference in the energy stored in the DC-link capacitor during the charging process. As such, storage capacitance energy ripple (E_r) can be written as [39], [40];

$$\Delta E_r = \frac{1}{2}c\,|v_{dc,max}|^2 - \frac{1}{2}c\,|v_{dc,min}|^2 \tag{49}$$

where the subscript $\min$ and $\max$ indicate the minimum and the maximum value while $\Delta E_r$is the energy variation in the energy storage capacitance. The energy storage capacitance in the DC-link can be written with reference to the energy variation, average and ripple voltages of the DC-link as follows:

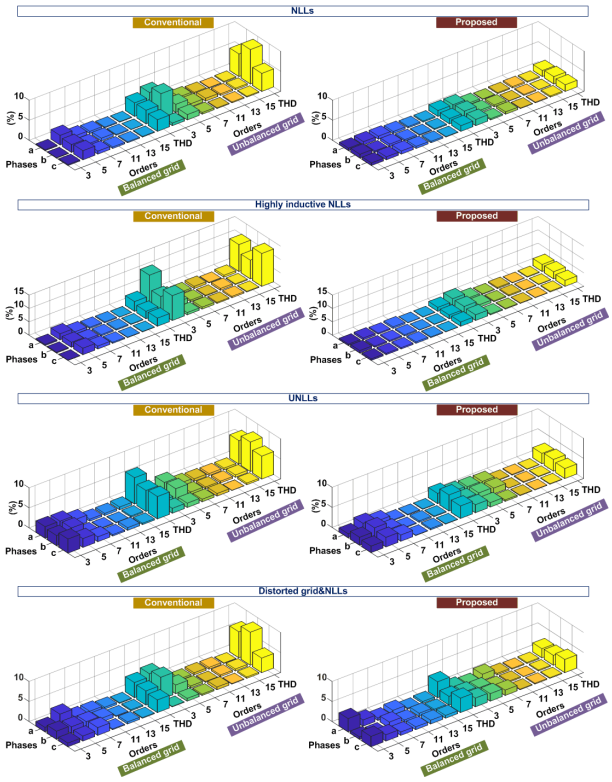

Figure 6. The current harmonic spectrum of conventional and proposed control algorithms under various cases.

$$c = \frac{\Delta E_r}{v_{dc,avg}\Delta\hat{v}_{dc}} \tag{50}$$

where $v_{dc,avg} = 0.5\left(|v_{dc,max}| + |v_{dc,max}|\right)$ and the ripple voltage in the DC-link is $\Delta\hat{v}_{dc} = |v_{dc,max}| - |v_{dc,min}|$. The ripple factor of this voltage (or utilization of the capacitor voltage) can be represented by voltage ripple and average voltage of the DC-link.

$$\eta_v = \Delta\hat{v}_{dc}/v_{dc,avg} \tag{51}$$

where η_v is the voltage ripple factor. The storage capacitance can be written by using (49), 50) and (51) as:

$$c = \frac{\Delta E_r}{\eta_v v_{dc,avg}}\left(\frac{\eta_v + 2}{2v_{dc,max}}\right)^2 \tag{52}$$

As depicted in Table III, three important features such as increasing and decreasing filter inductance and DC-link capacitance, and current tracking ability are considered to analyze the robustness of the method developed in this work. Although the filter inductance is increased or decreased by 20%, the current THD is around 1.47%. Besides, even with a DC-link capacitor increment and decrement of 30%, the voltage ripple variations changes slightly. Results in Table III indicate resilient performance by the developed method even under large variation of the filter inductance and DC-link capacitance values.

Table III
CURRENT THD AND VOLTAGE RIPPLES IN THE DC-LINK UNDER DIFFERENT FILTER INDUCTOR AND DC-LINK CAPACITOR VALUES.

ΔL	-20%	0	+20%
THD (Isa)	1.50%	1.47%	1.46%
Current tracking ability		Less affected	
c	-30%	Nominal	+30%
$\Delta\hat{v}_{dc}$	5.7V	4.1V	3.1V

V. CONCLUSION

With the growth of harmonics originated from by NLLs like EV battery chargers, the SAPF is considered as an effective solutions for the power quality improvement of operational EV charging stations hosting distribution network. A novel control strategy is conceived in this paper for high-performance operation of the SAPF under NLL, UNLL and highly inductive NLLs during grid voltage disturbances. The LKF with fast and good harmonic rejection capability has been utilized to extract load current harmonics and PCC voltages. One of the noteworthy contributions of this paper is to regulate and charge DC-link capacitor voltage with a Luenberger observer based ST-SMC, which ensures a constant DC-link voltage and contribute to generating sinusoidal source currents. Through quasi real-time study, it has been verified that the Luenberger observer based ST-SMC accomplishes fast dynamic response with 10ms convergence time and minimizes voltage ripples compared to PI control (having dynamic response of 40ms) and some other conventional methods in the literature. The developed control ensures very low DC-link ripple magnitude of 1V, while the conventional control has voltage ripple magnitude in the DC-link of nearly 6V. The controller developed in this work better regulates the individual harmonic amplitudes and lowers the THD in the current waveforms (less than 5%) as per the relevant IEEE standard. Balanced low THD (1.5%) sinusoidal currents are obtained through the proposed strategy. It has been found that the method developed in this work achieves a successful performance in compensating harmonics and ensures a fast dynamic response. The proposed control strategy provide distinct important features as opposed to most of the well-known conventional methods. As a future work, full real-time validation of the proposed control method will be considered.

REFERENCES

[1] M. Sharma, B. S. Rajpurohit, S. Agnihotri, and S. Singh, "Data analytics based power quality investigations in emerging electric power system using sparse decomposition," *IEEE Transactions on Power Delivery*, pp. 1–1, 2022.

[2] G. Sharma, V. K. Sood, M. S. Alam, and S. M. Shariff, "Comparison of common DC and AC bus architectures for EV fast charging stations and impact on power quality," *ETransportation*, vol. 5, p. 100066, 2020.

[3] J. M. Pattery, S. Jayaprakasan, E. P. Cheriyan, and R. Ramchand, "A composite strategy for improved power quality using micro compensators in secondary distribution systems," *IEEE Transactions on Power Delivery*, vol. 37, no. 2, pp. 1027–1035, 2022.

[4] H. T. Nguyen, A. S. Al Sumaiti, K. Al Hosani, K. Al Jaafari, Y.-J. Byon, J. Y. Alsawalhi, and M. S. El Moursi, "Enhanced performance of charging stations via converter control under unbalanced and harmonic

distorted grids," *IEEE Transactions on Power Delivery*, vol. 36, no. 6, pp. 3964–3976, 2021.

[5] T. Na, Q. Zhang, J. Tang, and J. Wang, "Active power filter for single-phase quasi-z-source integrated on-board charger," *CPSS Transactions on Power Electronics and Applications*, vol. 3, no. 3, pp. 197–201, 2018.

[6] G. Chang and T.-C. Shee, "A novel reference compensation current strategy for shunt active power filter control," *IEEE Transactions on Power Delivery*, vol. 19, no. 4, pp. 1751–1758, 2004.

[7] S. Rahmani, N. Mendalek, and K. Al-Haddad, "Experimental design of a nonlinear control technique for three-phase shunt active power filter," *IEEE Transactions on Industrial Electronics*, vol. 57, no. 10, pp. 3364–3375, 2010.

[8] Q.-N. Trinh and H.-H. Lee, "An advanced current control strategy for three-phase shunt active power filters," *IEEE Transactions on Industrial Electronics*, vol. 60, no. 12, pp. 5400–5410, 2013.

[9] S. Biricik, S. Redif, Ö. C. Özerdem, S. K. Khadem, and M. Basu, "Real-time control of shunt active power filter under distorted grid voltage and unbalanced load condition using self-tuning filter," *IET Power Electron.*, vol. 7, no. 7, pp. 1895–1905, 2014.

[10] S. Biricik and H. Komurcugil, "Three-level hysteresis current control strategy for three-phase four-switch shunt active filters," *IET Power Electron.*, vol. 9, no. 8, pp. 1732–1740, 2016.

[11] R. Panigrahi and B. Subudhi, "Performance enhancement of shunt active power filter using a Kalman filter-based H_∞ control strategy," *IEEE Transactions on Power Electronics*, vol. 32, no. 4, pp. 2622–2630, 2017.

[12] H. F. Farahani, A. Rabiee, and M. Khalili, "Plug-in electric vehicles as a harmonic compensator into microgrids," *Journal of Cleaner Production*, vol. 159, pp. 388–396, 2017.

[13] S. Taghizadeh, M. Hossain, J. Lu, and W. Water, "A unified multi-functional on-board ev charger for power-quality control in household networks," *Applied energy*, vol. 215, pp. 186–201, 2018.

[14] A.-H. M. Abu-Jalala, T. Cox, C. Gerada, M. Rashed, T. Hamiti, and N. Brown, "Power quality improvement of synchronous generators using an active power filter," *IEEE Transactions on Industry Applications*, vol. 54, no. 5, pp. 4080–4090, 2018.

[15] R. Chilipi, N. Al Sayari, K. Al Hosani, M. Fasil, and A. R. Beig, "Third order sinusoidal integrator (TOSSI)-based control algorithm for shunt active power filter under distorted and unbalanced voltage conditions," *International Journal of Electrical Power & Energy Systems*, vol. 96, pp. 152–162, 2018.

[16] G. Pandove and M. Singh, "Robust repetitive control design for a three-phase four wire shunt active power filter," *IEEE Transactions on Industrial Informatics*, vol. 15, no. 5, pp. 2810–2818, 2019.

[17] S. Jiao, K. R. Ramachandran Potti, K. Rajashekara, and S. K. Pramanick, "A novel DROGI-based detection scheme for power quality improvement using four-leg converter under unbalanced loads," *IEEE Transactions on Industry Applications*, vol. 56, no. 1, pp. 815–825, 2020.

[18] V. N. Jayasankar and U. Vinatha, "Backstepping controller with dual self-tuning filter for single-phase shunt active power filters under distorted grid voltage condition," *IEEE Transactions on Industry Applications*, vol. 56, no. 6, pp. 7176–7184, 2020.

[19] S. G. Basha, V. Mani, and S. Mopidevi, "Single-phase thirteen-level dual-boost inverter based shunt active power filter control using resonant and fuzzy logic controllers," *CSEE Journal of Power and Energy Systems*, pp. 1–16, 2020.

[20] S. Ouchen, M. Benbouzid, F. Blaabjerg, A. Betka, and H. Steinhart, "Direct power control of shunt active power filter using space vector modulation based on supertwisting sliding mode control," *IEEE Journal of Emerging and Selected Topics in Power Electronics*, vol. 9, no. 3, pp. 3243–3253, 2021.

[21] A. K. Dubey, J. P. Mishra, and A. Kumar, "Modified CCF based shunt active power filter operation with dead-band elimination for effective harmonic and unbalance compensation in 3-phase 3-wire system," *IEEE Transactions on Power Delivery*, pp. 1–1, 2021.

[22] O. Kukrer, H. Komurcugil, R. Guzman, and L. G. de Vicuna, "A new control strategy for three-phase shunt active power filters based on FIR prediction," *IEEE Transactions on Industrial Electronics*, vol. 68, no. 9, pp. 7702–7713, 2021.

[23] N. B. P, J. M. Guerrero, P. Siano, R. Peesapati, and G. Panda, "A novel modified control scheme in grid-tied photovoltaic system for power quality enhancement," *IEEE Transactions on Industrial Electronics*, vol. 68, no. 11, pp. 11 100–11 110, 2021.

[24] H. Komurcugil, S. Bayhan, N. Guler, and F. Blaabjerg, "An effective model predictive control method with self-balanced capacitor voltages for single-phase three-level shunt active filters," *IEEE Access*, vol. 9, pp. 103 811–103 821, 2021.

[25] M. Golla, S. Thangavel, K. Chandrasekaran, and S. P. Simon, "Real-time implementation of PV fed universal active power filter using CF-SOGI based IPBT control scheme," *Electr. Power Syst. Res.*, vol. 206, p. 107779, 2022.

[26] A. Meligy, T. Qoria, and I. Colak, "Assessment of sequence extraction methods applied to MMC-SDBC STATCOM under distorted grid conditions," *IEEE Transactions on Power Delivery*, pp. 1–1, 2022.

[27] F. Sevilmiş and H. Karaca, "Implementation of enhanced non-adaptive cascaded DSC-PLLs for renewable energy systems," *International Journal of Electrical Power & Energy Systems*, vol. 134, p. 107470, 2022.

[28] V. Monteiro and J. L. Afonso, "A unified topology for the integration of electric vehicle, renewable energy source, and active filtering for the power quality improvement of the electrical power grid: An experimental validation," *Electronics*, vol. 11, no. 3, p. 429, 2022.

[29] M. C. Rodrigues, I. D. Souza, A. A. Ferreira, P. G. Barbosa, and H. A. Braga, "Simultaneous active power filter and G2V (or V2G) operation of EV on-board power electronics," in *IECON 2013-39th Annual Conference of the IEEE Industrial Electronics Society*. IEEE, 2013, pp. 4684–4689.

[30] A. Ahmadi, A. Tavakoli, P. Jamborsalamati, N. Rezaei, M. R. Miveh, F. H. Gandoman, A. Heidari, and A. E. Nezhad, "Power quality improvement in smart grids using electric vehicles: a review," *IET Electr. Syst. Transp.*, vol. 9, no. 2, pp. 53–64, 2019.

[31] A. Levant, "Higher-order sliding modes, differentiation and output-feedback control," *Int J Control*, vol. 76, no. 9-10, pp. 924–941, 2003.

[32] X. Shen, J. Liu, A. Marquez, W. Luo, J. I. Leon, S. Vazquez, and L. G. Franquelo, "A high-gain observer-based adaptive super-twisting algorithm for DC-link voltage control of NPC converters," *Energies*, vol. 13, no. 5, p. 1110, 2020.

[33] H. Komurcugil, S. Biricik, S. Bayhan, and Z. Zhang, "Sliding mode control: Overview of its applications in power converters," *IEEE Industrial Electronics Magazine*, vol. 15, no. 1, pp. 40–49, 2021.

[34] M. Liserre, F. Blaabjerg, and S. Hansen, "Design and control of an LCL-filter-based three-phase active rectifier," *IEEE Transactions on Industry Applications*, vol. 41, no. 5, pp. 1281–1291, 2005.

[35] H. Deng, J. Fang, Y. Qi, Y. Tang, and V. Debusschere, "A generic voltage control for grid-forming converters with improved power loop dynamics," *IEEE Transactions on Industrial Electronics*, pp. 1–1, 2022.

[36] H. Vardhan, B. Akin, and H. Jin, "A low-cost, high-fidelity processor-in-the loop platform: For rapid prototyping of power electronics circuits and motor drives," *IEEE Power Electronics Magazine*, vol. 3, no. 2, pp. 18–28, 2016.

[37] S. Wu and Z. Liu, "Low-frequency stability analysis of vehicle-grid system with active power filter based on dq-frame impedance," *IEEE Transactions on Power Electronics*, vol. 36, no. 8, pp. 9027–9040, 2021.

[38] B. Xu, K. Liu, X. Ran, Q. Huai, and S. Yang, "Model predictive duty cycle control for three-phase Vienna rectifiers with reduced neutral-point voltage ripple under unbalanced DC links," *IEEE Journal of Emerging and Selected Topics in Power Electronics*, pp. 1–1, 2022.

[39] S. Li, A. T. L. Lee, S.-C. Tan, and S. Y. R. Hui, "Plug-and-play voltage ripple mitigator for DC links in hybrid AC-DC power grids with local bus-voltage control," *IEEE Transactions on Industrial Electronics*, vol. 65, no. 1, pp. 687–698, 2018.

[40] M. A. A. M. Zainuri, M. A. M. Radzi, A. C. Soh, N. Mariun, and N. A. Rahim, "DC-link capacitor voltage control for single-phase shunt active power filter with step size error cancellation in self-charging algorithm," *IET Power Electron.*, vol. 9, no. 2, pp. 323–335, 2016.